September 2015 ■ Volume 99 ■ Number 9

Official Journal of
The Transplantation Society &
International Liver Transplantation Society

Transplantation®

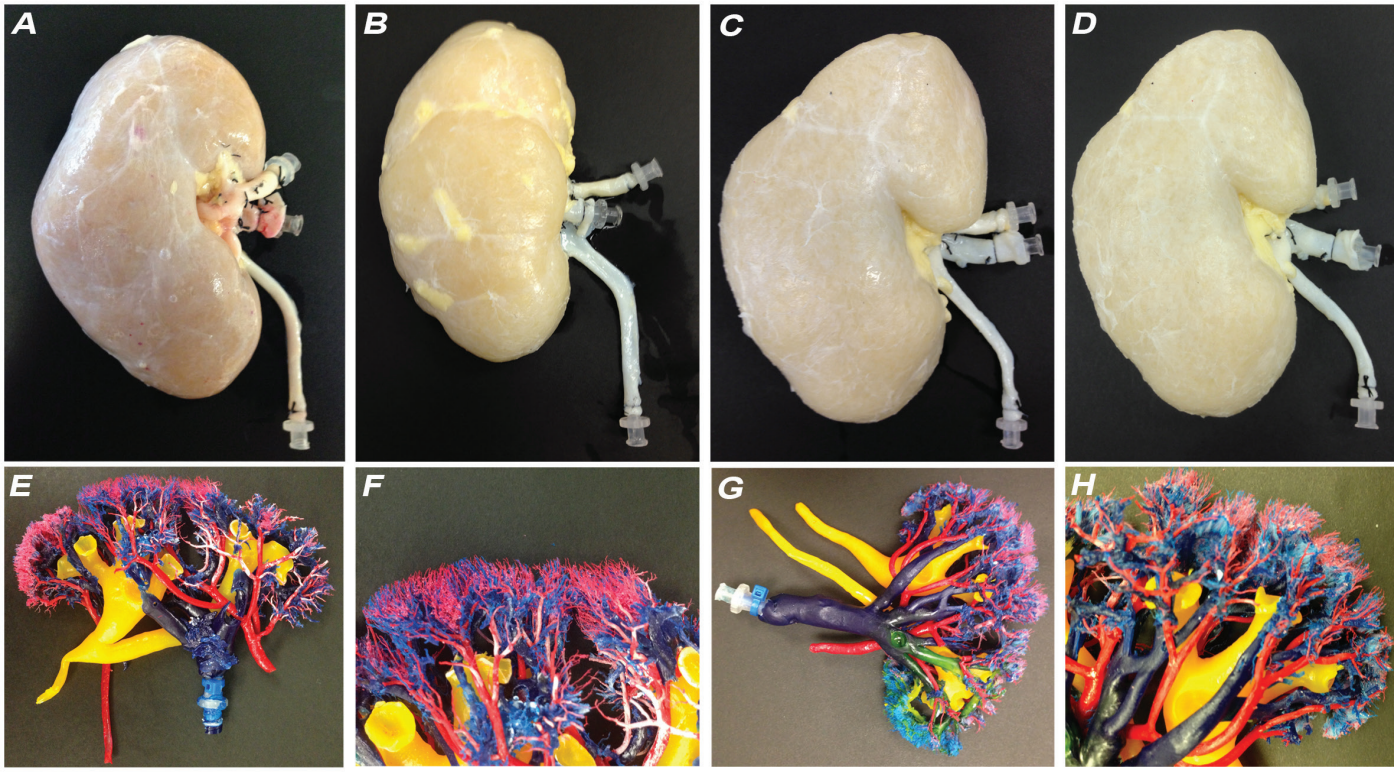

Wolters Kluwer

www.transplantjournal.com

- Renal ECM scaffolds from discarded kidneys
- Renal function and transplantation in liver disease
- Metalloproteinase profiling in lung transplant recipients with good outcome and BOS
- Impact of CMV on long-term mortality and cancer risk after organ transplantation

Renal ECM scaffolds from discarded kidneys maintain glomerular morphometry and vascular resilience, and retains critical growth factors

Andrea Peloso[1,2], Astgik Petrosyan[3], Stefano Da Sacco[3], Christopher Booth[1], Joao Paulo Zambon[1], Timothy O'Brien[4], Charles Aardema[5], John Robertson[1,4,5], Shay Soker[1], Robert J Stratta[1], Laura Perin[3], Giuseppe Orlando[1]

[1] Wake Forest School of Medicine, Winston Salem, NC, USA
[2] General Surgery, Fondazione IRCCS Policlinico San Matteo Pavia and University of Pavia, Pavia, Italy
[3] GOFARR Laboratory, Saban Research Institute, Children's Hospital Los Angeles; Department of Urology, University of Southern California, Los Angeles, California.
[4]Departments of Biomedical and Mechanical Engineering, Virginia Tech, Blacksburg, VA
[5] Smart Perfusion LLC, Denver, NC

Abbreviations: ECM extracellular matrix, hrECM human renal extracellular matrix, GFs growth factors

Pages:	References:
Main body word count:	Abstract word count:
Total word count:	Figures:

Address for correspondence:

Laura Perin, PhD
GOFARR Laboratory for Organ Regenerative Research and Cell Therapeutics, Saban Research Institute, Children's Hospital Los Angeles. Department of Urology, University of Southern California, Los Angeles, California, USA
LPerin@chla.usc.edu

Giuseppe Orlando, MD, PhD, Marie Curie Fellow
Department of General Surgery, Section of Transplantation, Wake Forest Baptist Health. Wake Forest Institute for Regenerative Medicine. Wake Forest School of Medicine, Winston-Salem, NC, USA.
gorlando@wakehealth.edu

Abstract

Extracellular matrix (ECM) scaffolds obtained through detergent-based decellularization of native kidneys, represent the most promising platform for investigations aiming at manufacturing kidneys for transplant purposes. We previously showed that decellularization of the human kidney yields renal ECM scaffolds (hrECMs) that maintain their basic molecular components, are cytocompatible, stimulate angiogenesis and show an intact innate vasculature. However, evidence that the decellularization preserves glomerular morphometric characteristics, physiological parameters (pressures and resistances of the vasculature bed) and biological properties of the renal ECM, including retention of important growth factors (GFs), is still missing. To address these critical issues, we processed hrECMs, originally destined to transplantation and eventually discarded. We demonstrated that our decellularization protocol allows preservation of the three-dimensional conformation of the native glomerulus, both morphologically and morphometrically. Using the resin casting approach and pulse-wave measurements, we determined that hrECMs maintain intact the microvasculature dimension and well as physiological function. Moreover, after decellularization, important GFs including VEGF and its receptors are retained in the matrices. Collectively, these results indicate that discarded human kidneys are a suitable source of renal scaffolds since they maintain a well preserved structure and function of the vasculature, as well as GFs that are fundamental to achieve a satisfying re-cellularization of the scaffold *in vivo* due to their angiogenic properties. Therefore, the use of hrECMs for kidney bioengineering applications may be more clinically applicable than kidneys derived from animals.

Introduction

Regenerative medicine has shown immense potential to address the limited number of transplantable organs and to allow immunosuppression-free transplantation, through the generation of body parts from patient's own biomaterials. Among the various approaches to organ bioengineering or regeneration, the seeding of cells on supporting scaffolding material – namely, cell-on-scaffold seeding technology (CSST)[2] – seems to offer the quickest route to clinical application. In fact, this technology has allowed the production of numerous, yet relatively simple body parts for therapeutic purposes, that were eventually implanted in more than 200 patients[1]

On the wake of these preliminary, yet groundbreaking achievements, CSST is being applied also to manufacture more complex, metabolic, transplantable organs, including the kidney. In particular, extracellular matrix (ECM) scaffolds obtained through the detergent-based decellularization of multiple species are used as a template for the seeding of kidney specific cells or progenitor cells, in the attempt to regenerate the parenchymal compartment, as well as of endothelial cells or progenitor cells aiming at the full regeneration of the endothelium. Since the very first report by Ross et al.[3] on the production of bioactive ECM scaffolds from rodent kidneys, several studies have followed[4-12] and have provided evidence that renal ECM scaffolds can be successfully and consistently produced from virtually all species including humans[9,13], are completely acellular and virtually non-immunogenic, maintain their architecture and essential molecular composition, lack cell membrane molecules, are able to determine cell phenotype and induce genes of renal development, possess remarkable angiogenic properties as demonstrated by the ability to induce vessel formation in the chorioallantoic membrane, are biocompatible in vitro and in vivo, and, when repopulated with renal cells, are able to show some function. Moreover, when acellular porcine renal ECM scaffolds are implanted in pigs, the framework of the innate vasculature remains well preserved and is able to well sustain physiologic blood pressure[4].

In order to validate these promising preliminary data in a more clinically relevant model, our group is applying CSST to human kidneys initially procured for transplant purposes, but eventually discarded due to various reasons[13]. In fact, in the United States, as more than 2600 kidneys are discarded annually from the total number of kidneys procured for transplantation, we hypothesized that this organ pool may be used as a platform for renal bioengineering and regeneration research. We showed that SDS-based decellularization yields consistently and successfully human renal ECM scaffolds (hrECMs) with a well-preserved three-dimensional architecture, an intact glomerular basement membrane along with other important structural proteins. Notably, our scaffolds lack HLA antigens and possess a striking ability to induce angiogenesis, which is an essential biological characteristic of any biomaterials in view of optimal, *ad hoc* re-cellularization and function following implantation *in vivo*.

Therefore, we conceived, designed and implemented the present study to complete the characterization of our hrECMs, by evaluating for the first time the microvasculature using the resin casting method, in addition to robustly assessing the dimension of the glomerular capillaries and arterioles. Moreover, in order to thoroughly assess the compliance and resilience of the framework of the innate vasculature within hrECMs, we measured the actual arterial and venous pressures within the framework of the vasculature of our matrices, with the use of a pulse-wave, set within the physiological limits. Finally, we evaluated the presence of soluble

growth factors (GFs) that possibly can be retained within the rhECMs and that are responsible for inducing angiogenesis.

Materials and Methods

Kidney procurement and preparation

Kidneys were procured for transplant purposes but then discarded for various reasons including anatomical abnormalities such as glomerulosclerosis, interstitial fibrosis, tissue inflammation or cortical necrosis. All organs were procured within the designated service area of our local procurement organization (Carolina Donor Service) and were refused by all local, regional, and national transplant centers. Kidneys were offered to the transplant team of the Wake Forest School of Medicine and processed at the Wake Forest Institute for Regenerative Medicine after the complete exhaustion of the national list.

Kidneys were received in sterile cold solution (saline solution NaCl 0.9%) and preserved until shipment. The aortic patch and the renal vein were prepared according to transplant protocol. The renal vein was dissected and sectioned at 2 cm from its origin. Multiple arteries were reconstructed in order to create a single arterial inlet. Peripheral fat and lymphatic tissue were ligated with 2/0 silk ties. Sixteen gauge intravenous catheters were inserted into the renal artery, the renal vein, and the ureter. The renal artery and the ureter were subsequently tested for possible leakages and eventually repaired with 6/0 Prolene sutures. Because all kidneys had been biopsied at the upper pole at the time of procurement, a renorrhaphy of the "wedge" defect was performed with 4-0 PDS suture in a running way. Kidneys were finally placed on ice until decellularization.

Kidney Decellularization and hrECMs production

The angiocatheters previously inserted in the renal artery and in the ureter were connected to a pump (Masterflex L/S peristaltic pump with Masterflex L/S easy load pump head and L/S 16G tubing, Cole-Palmer Instrument Co, Vernon Hills, IL, USA) to allow continuous rinsing with different solutions, starting with phosphate buffer saline (PBS) at the rate of 12 ml/min for 12h (8.640 mL total).

Afterward, 0.5% sodium dodecyl sulphate (SDS, Sigma-Aldrich, St. Louis, MO, USA)–based solution was delivered at the same flow rate for 48h (34.560 mL total) in both the renal artery and ureter. Finally the kidneys were rinsed with DNase (Sigma-Aldrich, St. Louis, MO, USA) for 6h at a flow rate of 6 ml/h and then with phosphate buffer saline, PBS (Sigma-Aldrich, St. Louis, MO, USA) at the same flow rate for 5 days (43.320 mL total). The histological characterization of the bioscaffolds was performed as previously described[13] in order to confirm absence of cellular residual (data not shown).

Resin vascular cast

Resin casting of the innate vasculature was obtained as previously described[14,15]. A total of 16 kidneys underwent resin vascular cast treatment divided into two different groups: group 1 counting eight native/cellular kidneys versus group 2 counting eight hrECMs. Precasting treatment was carried out via injection through arterial inlet of 60ml heparinized PBS solution in order to prevent any kind of blood clotting while washing out of the remaining blood from the vasculature tree. For each kidney, 60ml of specific casting resin was prepared by mixing 50ml of

casting resin monomer (Batson's #17 Monomer Base Solution Cat#02599, Polyscience, Inc., Warrington, PA, USA), 10ml of catalyst (Batson's #17 Anatomical Corrosion Kit Promoter Cat# 02610, Polyscience, Inc., Warrington, PA, USA) and 10 drops of promoter (Batson's #17 Catalyst Cat# 02608, Polyscience, Inc., Warrington, PA, USA). This solution was then slowly injected through the renal artery (15-20 ml colored by red dye, Batson's #17 Anatomical Corrosion kit Red dye Lot #533945, Polyscience, Inc., Warrington, PA, USA) the renal vein (15-20 ml colored by blue dye, Batson's #17 Anatomical Corrosion kit Blue dye Lot #623514, Polyscience, Inc., Warrington, PA, USA) and the ureter (10-15 ml colored by yellow dye, Batson's #17 Anatomical Corrosion kit Yellow dye Lot #623514, Polyscience, Inc., Warrington, PA, USA). After the onset of polymerization kidneys were placed in deionized water overnight and then all the tissue was cleared by two alternating rinses (24h each) with 10% and 5% of hydrochloric acid respectively.

Scanning Electron Microscopy (SEM)

Five 5x5x5mm samples were obtained from each kidney cast (a total of eighty samples, forty from group 1 and forty from group 2) in randomly selected areas of the cortex simply cutting them out with microsurgical scissors. These samples were mounted on silver plates sputter coated with gold and analyzed by Scanning Electron Microscopy (SEM) at 15KV (Hitachi S-2600N Scanning Electron Microscopy, Hitachi, Chiyoda, Tokyo, Japan). From each samples two three-dimensional images of the afferent artery and the glomeruli were taken (for a total of 160 glomerular images captured). All of the images were then analyzed by Image-J software (http://rsb.info.nih.gov/ij/). Afferent artery diameter was measured at three different points and averaged for statistical analysis. Glomerular diameter measured in the long and short axis and subsequently averaged. Modeling each glomerulus as a sphere, we used these diameter averages to calculate volume ($4/3\ \Pi r^3$). Six randomly selected glomerular capillaries from each image were measured and used to calculate average capillary diameter. From these data we evaluated the morphological properties of the glomeruli and their afferent arteries.

Determination of machine-perfusion vascular responsiveness

Nine donated human kidneys were machine-perfused at 4^oC for 12 hours with modified Krebs solution, using a unique cardioemulation perfusion technology (VasoWave®, Smart Perfusion, Denver, NC). This system produces a cardioemulating pulse wave to generate physiological systolic and diastolic pressures and flow rates within the organ. The system is capable of controlling the oxygen content of the perfusate above and below physiological norms. During perfusion, arterial pressure measurements were taken. A comparison was made between machine-set pressures (systolic/diastolic) and actual pressures within organs under perfusion. Organs with intact vasculature replicate an elastic response to machine-set pressures. Following decellularization, scaffolds from the same set of nine human kidneys were again machine-perfused (modified Krebs solution at 4^oC, for 12 hours) and arterial pressure measurements were taken as described. It is important to note that, if scaffolds had been damaged by de-cellularization, they would not elastically respond to machine-set pressures, and would leak fluid and would fail to sustain pressurization. Pressure measurements were collected for both cellularized and decellularized kidneys at a rate of 100/second and then sampled every 1000 points to create mean summary data.

Growth factor retention

5 hrECMs and 5 samples of native kidneys before decellularization were used to evaluate growth factor retention. Samples were procured with a 7 mm biopsy punch, stored in sterile PBS with 2% pen/strep (Hyclone Pe/Strep solution, Fisher Scientific, Waltham, MA, USA) and then shipped to the manufacturer (Raybiotech, http://www.raybiotech.com/) and processed accordingly. Specifically, tissue biopsies underwent homogenization by sonication in RayBiotech's proprietary lysis buffer (500 µL of lysis buffer per 10 mg tissue) and centrifugation for 5 minutes at 10,000 x g. Supernatants were then collected and assayed immediately or frozen for future use. Protein expression profiles were collected using the RayBio® Human Growth Factors Antibody Array G series 1, a custom glass chip-based multiplex ELISA array which measures 40 cytokines simultaneously. The tissue supernatants were incubated with the array chips after a blocking step and these were washed to remove nonspecific proteins, and biotin-labeled detection antibodies were added. The cytokine-antibody-biotin complexes can then be visualized through the addition of a HiLyte Fluor 532™ dye-labeled streptavidin. Spot intensities extracted from the scanned array image were normalized to positive controls included within each array. Average fluorescent intensity was obtained from duplicate signal intensities, adjusted to remove background and normalized to a positive control to account for differences among sub-arrays.

Immunofluorescence to assess maintenance of structural specific hrECMs components

In order to evaluate the presence of specific hrECM proteins, 1cm³ biopsies taken from the cortex of decellularized human kidneys were fixed in 10% formalin (Azer scientific, PA) for 2 hrs. After fixation samples were dehydrated in alcohol gradients and placed in toluene (Sigma-Aldrich, St. Louis, MO) for 30 min. Samples were kept overnight in a 50:50 toluene paraffin mixture. They were next changed into paraffin for 2 hours and later embedded. 5µm thick sections (Rotary Microtome -Leica, Rotary Microtome RM2235) were deparaffinized and rehydrated in alcoholic gradients for histology. Immunofluorescence analysis was conducted by overnight incubation with primary antibodies Collagen IV (ABCAM, Cambridge, MA 1:100), VEGFR-2 (ABCAM, Cambridge, MA 1.5:100), VE-Cadherin (ABCAM, Cambridge, MA 1.5:100) followed by 30 minute incubation with secondary anti-mouse or anti-rabbit Alexa Fluor 555 (Life Technologies Grand Island, NY 1:500). DAPI mounting (Vector Laboratories Burlingame, CA) was used to visualize samples with a Leica DM5500 B Microscope System.

Statistics

All graphical data are displayed as the mean + SEM. Statistical analysis was performed using Student's T-test and MatLab Software in order to compare measurements of glomeruli, arterioles and capillaries between the two experimental groups as well as the machine-perfusion vascular responsiveness. A p value less than 0.05 was considered statistically significant.

Results

Cast preparation and Morphometric Analysis

The resin filled the framework of the innate vasculature throughout the whole parenchyma, ultimately producing a high-fidelity 3D casting, as shown in Figure 1A-D. Our corrosion cast protocol successfully produced 16 satisfactory whole-kidney casts (8 native kidneys and 8 scaffolds), with uniform representation of the vascular network and glomeruli through the entire cortex, as shown in Figure 1E-H.

Five biopsies were taken from each organ and scaffold. Of each biopsy, five SEM images of randomly selected glomeruli were captured and studied (Figure 2). Morphometrical endpoints were: sagittal and transversal glomerular diameter (green lines); diameter of the afferent artery (red lines); diameter of six different glomerular capillaries, randomly selected (yellow lines). Results are shown synoptically in Figure 3. The average afferent arteriolar diameter was 24.20±0.49µm in native kidneys versus 23.65±0.63µm in hrECMs (p=n.s.). The average glomerular diameter was 224.37±5.23µm in the native kidneys versus 182.93±3.8µm in the scaffolds ($p<0.01$). Volumetric calculations were carried out using these figures by modeling glomeruli as spheres; analysis showed that volume of native glomeruli was statistically higher that in the hrECMs (7.17x10^6 +- 6.62 x10^5μm^3 versus 3.81 x10^6 +- 3.07 x 10^5 μm^3, $p<0.01$). Mean capillary width was 11.36±0.20 µm for native kidneys and 11.37±0.20 µm for renal scaffolds (p=n.s.). The mean afferent arteriolar diameter was 24.20 ± 0.64 µm for native kidneys and 23.65±0.72 µm for renal scaffolds (p=n.s.).

Machine-perfusion vascular responsiveness

In order to evaluate the effects of decellularization, we measured the vascular relasticity and ability to sustain pressure in both intact (pre-decellularization) and processed (post-decellularization) kidneys. To accomplish this, we connected the VasoWave perfusion system to the arterial and venous vessels and the applied pulsing, while measuring pressure responsiveness and fluid load in the closed loop system. Machine-perfused kidneys and hrECMs stabilized within 20 minutes of anastomosis and were effectively perfused in a closed-circuit system using 1-1.5L of modified Krebs solution for 12 hours. No interstitial edema or swelling was noted and there was no fluid 'weeping' from the surfaces or under the capsule of the experimental groups.

As shown in Figure 4A and 4B, the vasculature of both native kidney and hrECM demonstrated an elastic response to machine-set pressures. With a machine-set systolic pressure of 90 mmHg, the mean vascular elastic response of the native organ (measured by the difference of set versus actual pressure) was 0.898%. The mean vascular elastic response of the native organ to the diastolic (50 mmHg) pressure wave was 7.47%. Of note, administration of the arterial pressure wave temporally resulted in slightly higher actual arterial pressures, due to arterial dilation opposed by tissue pressure and venous backpressure. This is commonly seen as a manifestation of vascular resistance in normal kidneys.

Following decellularization, vascular elastic responses were again evaluated in the same 9 kidneys. With a machine-set systolic pressure of 90 mmHg, the mean vascular elastic response of the hrECMs (measured by the difference of set versus actual pressure) was 1.76%. There was no temporal rise in actual arterial pressure, demonstrating that decellularization effectively removed tissue backpressure. The mean vascular elastic response of the hrECMs to the diastolic (50 mmHg) pressure wave was 2.48%. Removal of cellular material did not compromise elastic response of the vascular scaffold. In fact, smoothing of elastic response was indicative of more effective perfusion (less difference in the diastolic mean deviation from the machine-set pressure wave).

Growth factor analysis

The multiplex array shows hrECMs retain numerous GFs that play vital role during important biological processes, including angiogenesis, renal development and regeneration, as well as glucose homeostasis (Figure 5 and Table 1). Immunofluorescence confirmed the

presence of collagen IV, VEGF-R2, as well as Ve-Cad (Figure 5B-D) within the hrECMs, indicating the preservation of the glomerular basement membrane and the presence of key molecules that support the capillaries structure within the glomeruli.

Discussion

The present study was conceived and designed to address critical, yet unaddressed aspects of ECM characterization, namely the integrity and resilience of the innate vasculature through vessel morphometry and perfusion studies, and the ability of hrECMs to retain GFs through direct quantification of a custom made panel of relevant GFs and ad hoc "in tissue" staining. Our findings show that the framework of the innate vasculature of hrECMs is well preserved and retains its innate resilience, and that GFs that are key players in critical processes of tissue development like angiogenesis remain within the matrix post decellularization at significant concentrations.

In regenerative medicine, CSST has shown the greatest potential to clinical translation, allowing the production of body parts bioengineered from patient's cells that were eventually implanted in more than 200 patients without any anastomosis to the recipient's vasculature, at the time of implantation. Instead, more complex metabolic organs like the kidney do require re-anastomosis between the vascular pedicle of the bio-artificial organ and the recipient's bloodstream, to allow function. Therefore, the acellular framework of the innate vasculature endowed within ECM scaffolds used for tissue engineering purposes should maintain the basic characteristics and resilience of the intact counterpart, in order to allow implantation and sustain physiological blood pressure *in vivo*. Moreover, as one of the critical functions of ECM in mammals is to act as reservoir for GFs to be released following specific stimuli[16], ECM scaffolds used for tissue engineering purposes ideally should maintain GFs. As hrECMs were proven to have the ability to induce the formation of new vessels in the *in ovo*[13] bioassay, there is evidence that several molecules involved in the inflammatory and angiogenesic cascades are present in the matrix post decellularization, demonstrating that our matrices are bioactive and so may facilitate the regeneration and re-building of new tissue after recellularization and ultimately implantation.

We conducted a morphometric study of the framework of the innate vasculature through 3D analysis of SEM images of corrosion casting, as described by Pereira-Sampaio et al. and Manelli et al. Analysis and measurement of casting imaging at SEM revealed that morphology and dimensions of the acellular glomerulus and its vascular network are relatively well-preserved post decellularization and are comparable to their cellular counterparts. We found that the diameter and volume of the glomerular macrovasculature within the hrECMs are contracted when compared with the normal kidney; this finding may possibly due to the absence of cells, accounting for a significant part of the whole volume of the intact, cellular glomerulus. Instead, we detected no significant differences in the width of glomerular capillaries and the branching pattern and integrity of the larger vessels. Overall, these data corroborate the idea that our decellularization method yield hrECMs that have the framework of the vascular network preserved at all hierarchical levels, namely large vessel (data not shown) and small cortical vessels. It should be emphasized that the preservation of an intact vascular bed in our hrECM is very important since the *sine qua non* for using innate scaffolds *in vivo* crucially depends on an intact vascular network that is able to sustain physiological blood pressure and perfusion as we alr4eady demonstrated in the porcine model[4]. Clearly, in regards to the decreased glomerular diameter and volume observed in our matrices, it is reasonable to hypothesize that the

regeneration of the endothelium would normalize those values (=bring them to values observed in the innate, cellular kidney).

Next, as the kidney is one of the major control stations of intravascular blood pressure, we wanted to determine whether the intact framework of the vascular network of hrECMs does maintain function and resilience, namely its ability to respond to changes in intravascular pressure. To do so, we used a state of the art technology that provided both a cardioemulating, physiologic pulse pressure and the ability to dynamically measure applied pressure and elastic vascular resistance for each pulse wave. Our analysis of pulse wave data and response to pressurization demonstrated that, although the process of decellularization removed cells, the scaffolds demonstrated the same elastic response characteristic of intact vascular beds. Specifically, scaffolds did not leak (no fluid wept from the surface) during perfusion and elastic rebound in response to an applied pulse wave was seen, although slightly diminished when compared to intact, cellularized kidneys.

To finalize the characterization of our matrices and determine whether they have the characteristic of implantable organs and induce formation of new vessels, we studied the GFs content of hrECMs. It is important to emphasize that, during kidney development as well as in the natural history of chronic kidney diseases, important GFs secreted and retained within the ECM orchestrate very complex cell-cell and cell-matrix interactions. For example variation in concentration of several growth factors including TGF-α, HB-EGF, IGF, and FGF are responsible for cell migration, proliferation, differentiation, induction of pro-fibrotic processes as well as possible pro-healing signaling with scar resolution[17]. Therefore, as GFs play a major role in determining progression or blockade of kidney damage, it is of vital importance to determine if the decellularization process of human kidneys preserves important stimuli that could eventually facilitate cellular repopulation and mediate induction of fibrosis, in future in vivo applications. Interestingly, we observed that several GFs, including TGF-α, FGF-6, IGFBP-3, HB-EGF, IGFBP-6, NT-3, P1GF, TGF-β, VEGF, and VEGF-D are present within our hrECMs. We confirmed the presence of critical transmembrane glycoproteins, namely Ve-cadherin and VEGFR-2, which are vital for the function and the strength of the endothelium and for the maintenance of glomerular endothelial cells fenestrations, essential for the glomerular barrier filtration. For example, VEGFR-2 postnatal deletion demonstrates a global defect in the glomerular microvasculature and the paracrine VEGF–VEGFR-2 signaling loop is identified as a critical component in the developing and in the filtering glomerulus[18]. The presence of these GFs should not be underestimated, showing that hrECMs provides not only structurally supportive vasculature, but also maintains architecturally specific transmembrane glycoproteins for glomerular endothelia cell function and support. Further investigations using cell seeding will be performed in order to determine the influence of these GFs on endothelial cellular fate. Nevertheless, these preliminary important data reveal, for the first time, that hrECMs is a possible candidate for tissue engineering purposes and posses all the necessary characteristics to induce functional vasculature *in vivo*.

To conclude, the present study demonstrates that the framework of the innate vasculature of hrEMCs is maintained at all hierarchical levels, is resilient and can sustain intravascular pressures comparable to what is observed in normal physiology. Also, hrECMs retains numerous GFs that are necessary for the maintenance of the endothelial cell homeostasis and function. This is information that may be critical for devising strategies aiming at the regeneration of the cellular compartment and *in vivo* implantation of bioengineered renal organoids for transplant purposes.

References

1. Orlando G, Soker S, Stratta RJ. Organ bioengineering and regeneration as the new Holy Grail of organ transplantation Ann Surg. 2013 Aug;258(2):221-32.
2. Salvatori M, Peloso A, Katari R, Zambon JP, Soker S, Stratta RJ, Orlando G. Semi-xenotransplantation: the regenerative medicine based-approach to immunosuppression-free transplantation and to meet the organ demand. Xenotransplantation 2014, July 8, ahead of print.
3. Ross EA, Williams MJ, Hamazaki T, Terada N, Clapp WL, Adin C, et al. Embryonic stem cells proliferate and differentiate when seeded into kidney scaffolds. J Am Soc Nephrol 2009;20:2338-47.
4. Orlando G, Farney A, Sullivan DC, AbouShwareb T, Iskandar S, Wood KJ, et al. Production and implantation of renal extracellular matrix scaffolds from porcine kidneys as a platform for renal bioengineering investigations. Ann Surg 2012;256:363-70.
5. Nakayama KH, Batchelder CA, Lee CI, Tarantal AF. Decellularized rhesus monkey kidney as a three-dimensional scaffold for renal tissue engineering. Tissue Eng Part A 2010;16(7):2207-16.
6. Nakayama KH, Batchelder CA, Lee CI, Tarantal AF. Renal tissue engineering with decellularized rhesus monkey kidneys: age-related differences. Tissue Eng Part A 2011;17(23-24):2891-901.
7. Nakayama KH, Lee CC, Batchelder CA, Tarantal AF. Tissue specificity of decellularized rhesus monkey kidney and lung scaffolds. PLoS One 2013;8(5):e64134.
8. Sullivan DC, Mirmalek-Sani SH, Deegan DB, Baptista PM, Aboushwareb T, Atala A, Yoo JJ. Decellularization methods of porcine kidneys for whole organ engineering using a high-throughput system. Biomaterials 2012;33(31):7756-64.
9. Song JJ, Guyette JP, Gilpin SE, Gonzalez G, Vacanti JP, Ott HC. Regeneration and experimental orthotopic transplantation of a bioengineered kidney. Nat Med 2013;19(5):646-51.
10. Bonandrini B, Figliuzzi M, Papadimou E, Morigi M, Perico N, Casiraghi F, Dipl C, Sangalli F, Conti S, Benigni A, Remuzzi A, Remuzzi G. Recellularization of well-preserved acellular kidney scaffold using embryonic stem cells. Tissue Eng Part A 2014;20(9-10):1486-98.
11. Wang Y, Bao J, Wu Q, Zhou Y, Li Y, Wu X, Shi Y, Li L, Bu H. Method for perfusion decellularization of porcine whole liver and kidney for use as a scaffold for clinical-scale bioengineering engrafts. Xenotransplantation. 2014 Oct 7 [Epub ahead of print].
12. Choi SH, Chun SY, Chae SY, Kim JR, Oh SH, Chung SK, Lee JH, Song PH, Choi GS, Kim TH, Kwon TG. Development of a porcine renal extracellular matrix scaffold as a platform for kidney regeneration. J Biomed Mater Res A. 2014 Jul 16 [Epub ahead of print].
13. Orlando G, Booth CL, Wang Z, Totonelli G, Ross CL, Moran E, Salvatori M, Maghsoudlou P, Turmaine M, Delario G, Al-Shraideh Y, Farooq U, Farney AC, Rogers J, Iskandar SS, Burns A, Marini FC, De Coppi P, Stratta RJ, Soker S. Discarded human kidneys as a source of ECM scaffolds for kidney regeneration technologies. Biomaterials 2013;34:5915-25.
14. Pereira-sampaio MA, Henry RW, Favorito LA, Sampaio FJ. Cranial pole nephrectomy in the pig model: anatomic analysis of arterial injuries in tridimensional endocasts. J Endourol. 2012;26(6):716-21.
15. Manelli A, Sangiorgi S, Binaghi E, Raspanti M. 3D analysis of SEM images of corrosion casting using adaptive stereo matching. Microsc Res Tech. 2007;70(4):350-4.
16. Hynes RO. The extracellular matrix: not just pretty fibrils. Science. 2009 Nov 27;326(5957):1216-9.

17. Jain RK, Au P, Tam J, et al. Engineering vascularized tissue. Nat Biotechnol. 2005;23(7):821-3.
18. Rahimi N, Kazlauskas A. A role for cadherin-5 in regulation of vascular endothelial growth factor receptor 2 activity in endothelial cells. Mol Biol Cell. 1999;10:3401–3407.

Figure 1. Whole human kidney decellularization and vascular corrosion cast. Figure **1A-D** shows kidney macroscopic frontal view during whole-kidney detergent-based decellularization protocol. Representative time lapse of kidney decellularization at T0 (**A**) and after 16, 32, and 48 hours (T1, T2 and T3) (**B**, **C** and **D**, respectively). It is noticeable that peristaltic perfusion through the renal artery and the ureter (12.5 ml/min), with the renal vein used as vascular outlet, permits homogeneous and complete cellular compartment removal with a slow progressive change of the color of the organ. Figure **1E-H** shows a human renal vascular corrosion cast obtained by injection of a specific resin via the renal artery (red dye), the renal vein (blue dye) and the ureter (yellow dye). Macroscopic anterior view of the endocast (**E**) shows the uniform distribution of the resin, obtained by a gentle continuous injection, inside the native kidney vascular tree from the renal hilum to last vascular branching. Panel F shows the 3D endocast of final renal vascular branching system; the resin filled the finest branches of the vascular network (arterial and venous). Panel G shows the complete preservation of the macrostructures of the organ (arterial, venous and ureteral collecting system). Interestingly, the sample in question possesses a double-ureter and pelvicaliceal system that preserves its entire structure at all detectable hierarchical levels. Even without cells present, the casting resin filled the whole scaffold in its upper and lower pole, producing a final high- fidelity tridimensional reconstruction. Magnification of the lower pole of the endocast (**H**) shows preservation of the final vascular divisions of the scaffold as observed from the native organ.

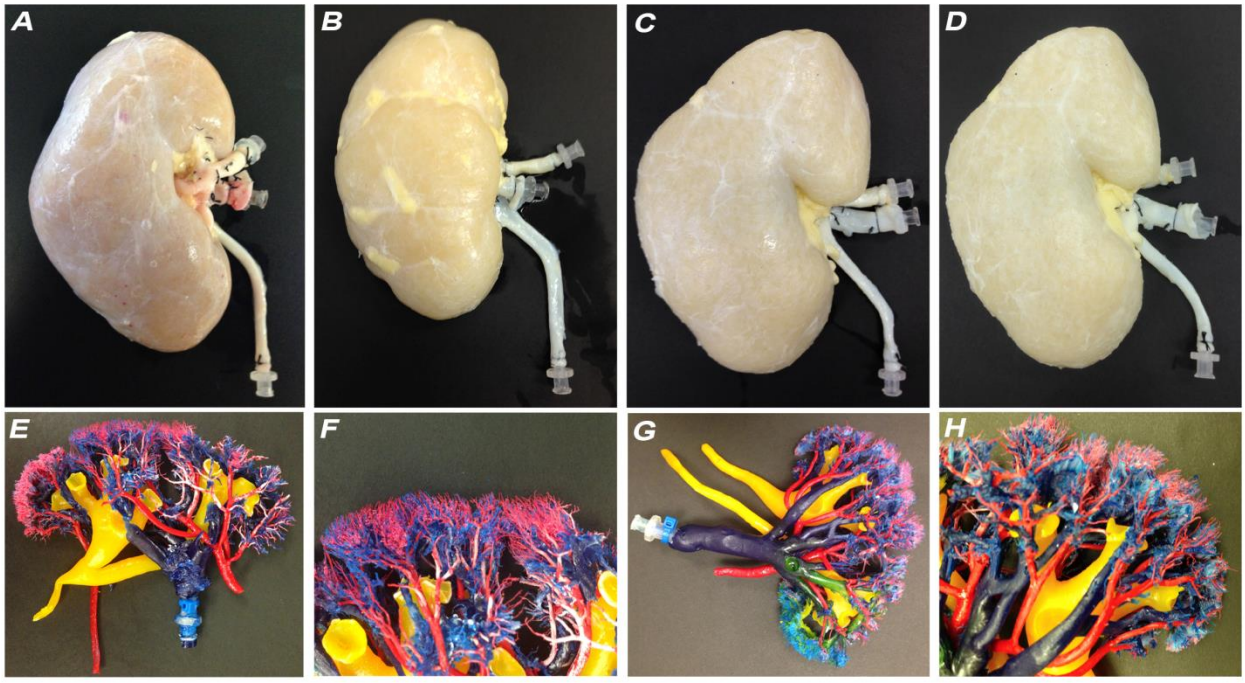

Figure 2. **Glomerular Scanning Electron Microscopy -SEM- morphometric analysis.** Figure **2A** and **2C** show representative SEM images of a single extracted native glomerulus derived from the cortical portion of the vascular corrosion endocast of a native kidney, while Figure **2B** and **2D** show representative SEM images of a single extracted glomerulus derived from the cortical portion of the vascular corrosion endocast of an acellular kidney (scalebar: 100 μm). In both series major glomerular components (afferent artery and branched capillaries) are clearly visible. Background from the original snapshot (**A** and **B**) was removed to enhance and highlight effective glomerular morphological shape and to more accurately extrapolate its morphometric measurements. Diameter was measured twice, sagittally and transversally, (**C** and **D**) and then the average was calculated (green lines and circle). Afferent arteriolar width was acquired from three different transversal points (red lines) (**C** and **D**) and the final average assessed. Finally six different transversal measurements were obtained (yellow lines) from singular capillaries in several areas of the glomerulus (**C** and **D**).

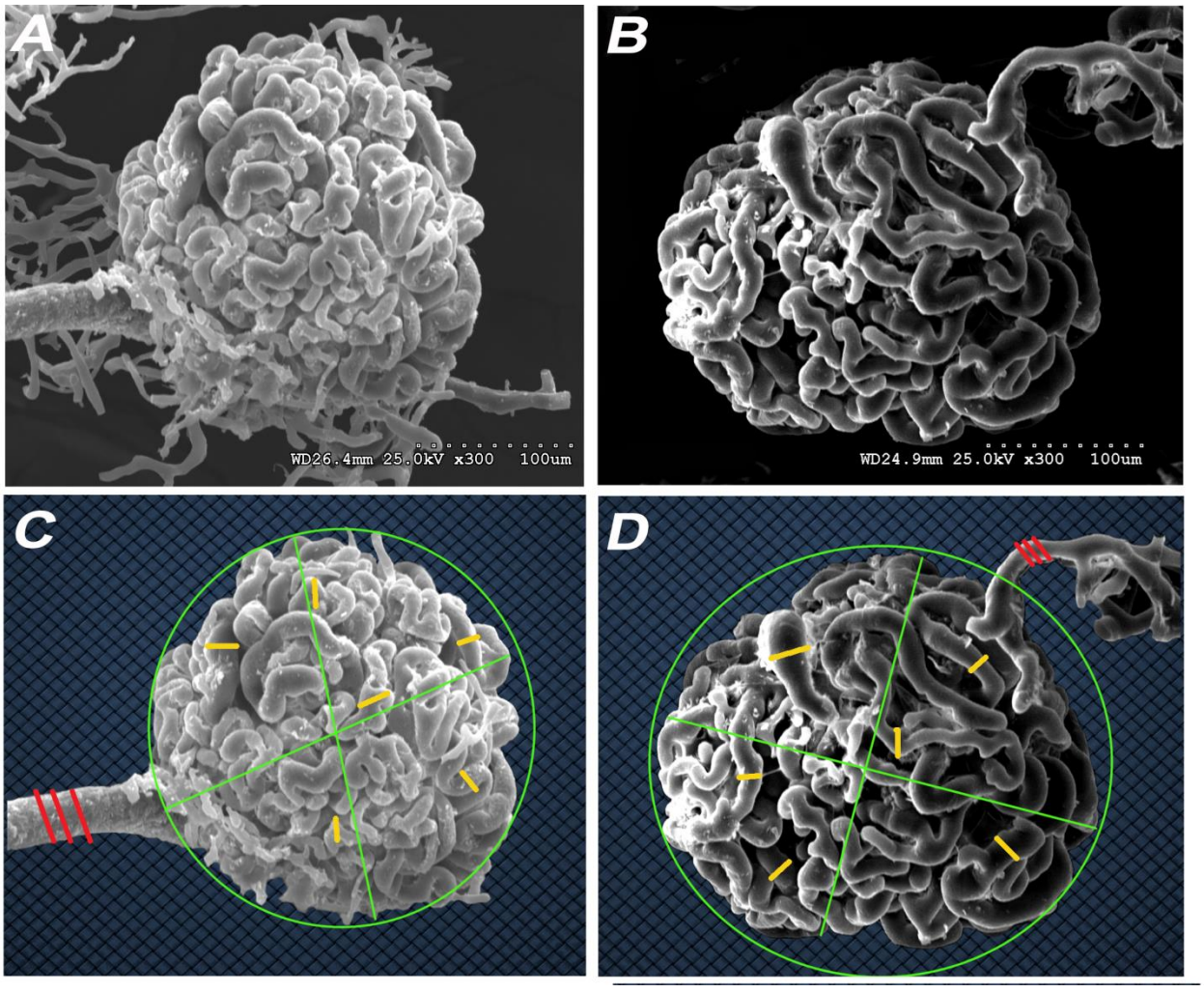

Figure 3. Morphometric analysis of native and decellularized glomeruli. The graphs present in Figure 3 exemplify the mean measurements expressed in um and um^3, of glomerular diameter (**A**), glomerular volume (**B**), afferent arteriolar diameter (**C**) and glomerular capillary with between 80 glomeruli derived from native kidney cast samples and 80 decellularized glomeruli derived from kidney cast samples. While glomerular diameter and volume significantly decrease in after decellularization, no change was noticed in arteriolar and capillary dimensions before and after decellularization. ** p< 0.01.

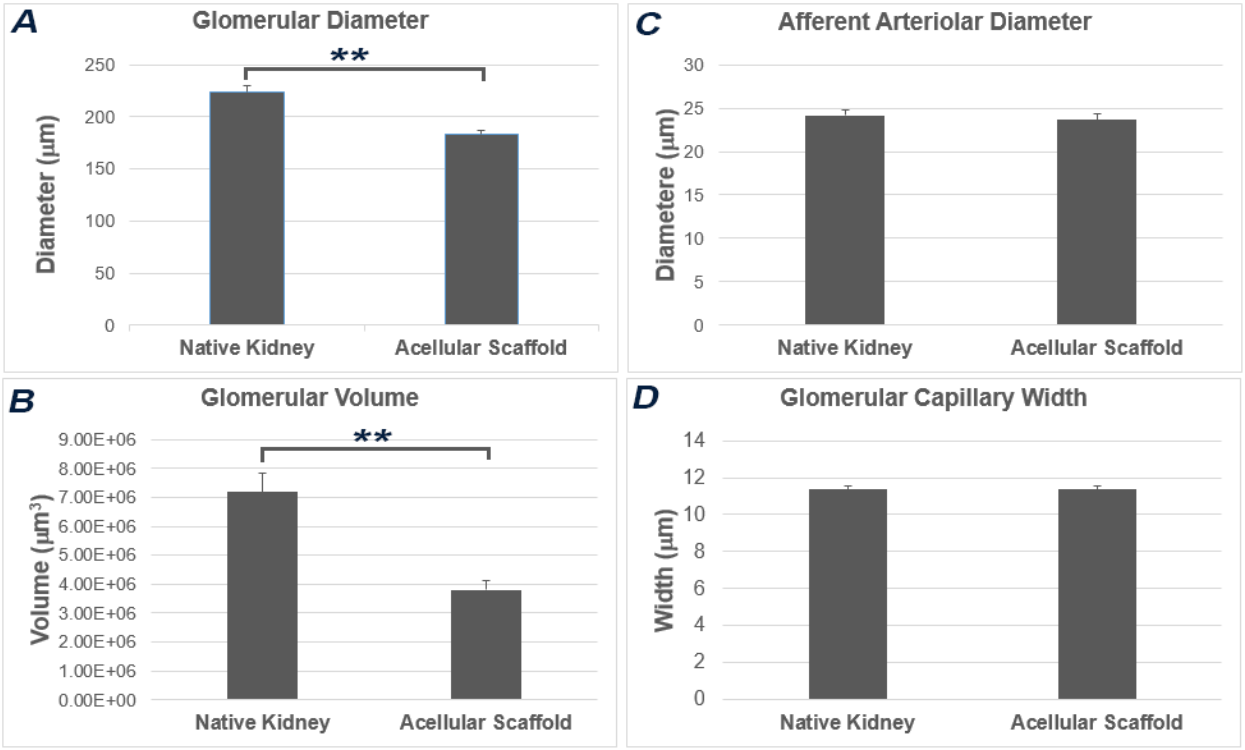

Figure 4. Measurement of mean systolic (Max) and diastolic (Min) pressure responsiveness. Panel A shows the measurement of mean systolic pressure responsiveness of nine human kidneys (before and after decellularization) machine-perfused at 90 mmHg for 12 hours. Points represent the % difference in the machine-set pressure and actual pressure. Native kidney, (blue line) and decellularized kidney, hrECMs (orange line) demonstrated an elastic response to machine set pressures (black line). The mean vascular elastic response in the native kidney was 0.898% versus 1.76% after decellularization. Panel B shows the measurement of mean diastolic pressure responsiveness of nine human kidneys (before and after decellularization) machine-perfused at 50 mmHg for 12 hours. Points represent the % difference in the machine-set pressure and actual pressure. Native kidney (blue line) and decellularized kidney, hrECMs (orange line) demonstrated an elastic response to machine set pressures (black line). The mean vascular elastic response in the native kidney was 7.47% versus 2.48 % after decellularization. Presence of an elastic rebound in response to the applied pulse wave confirmed that decellularization diminished but did not compromise the elastic response of the vascular scaffold.

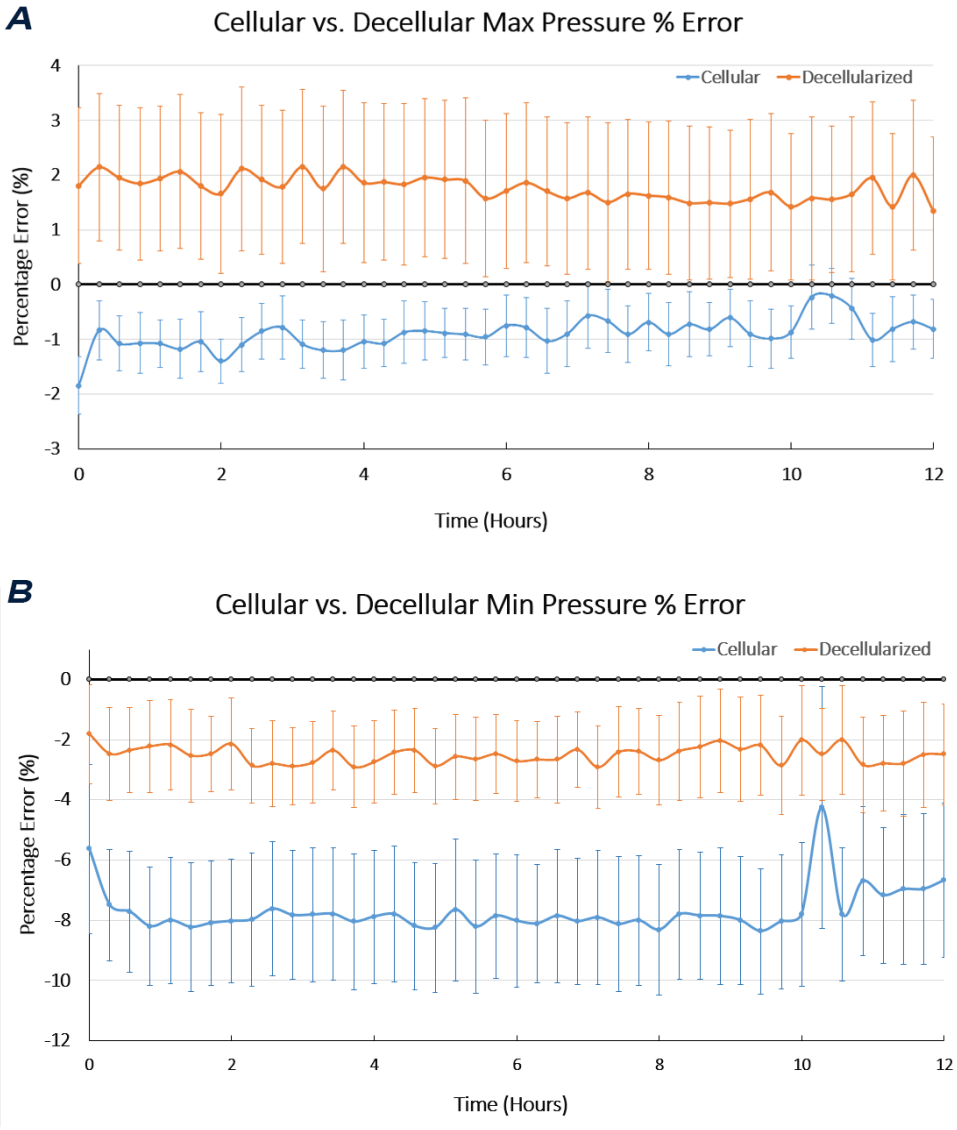

Figure 5. GFs retention within hrECMs and ad hoc immunofluorescence analysis. Panel A shows the results of a semi-quantitative analysis of the protein expression profile of different GFs measured within the decellularized kidney (hrECMs) using a custom RayBio® Human Growth Factors Antibody Array G series 1. Average fluorescent intensity was obtained from duplicate signal intensities, adjusted to remove background and normalized to a positive control to account for differences among sub-arrays. As a general trend, important molecules like TGFβ, IGFII, members of the TGF family and VEGF family are retained within the decellularized matrix. Immunofluorescence for collagen V (**B**, 20X), vascular endothelial growth factor receptor 2 (VEGFR2, **C**, 20X) and Ve-Cadherin (**D**, 20x) demonstrate that the decellularized glomeruli maintain the presence of important fibrous protein (collagen V) as well as VEGFR2 and Ve-Cadherin that are necessary for endothelial cell attachment and function.

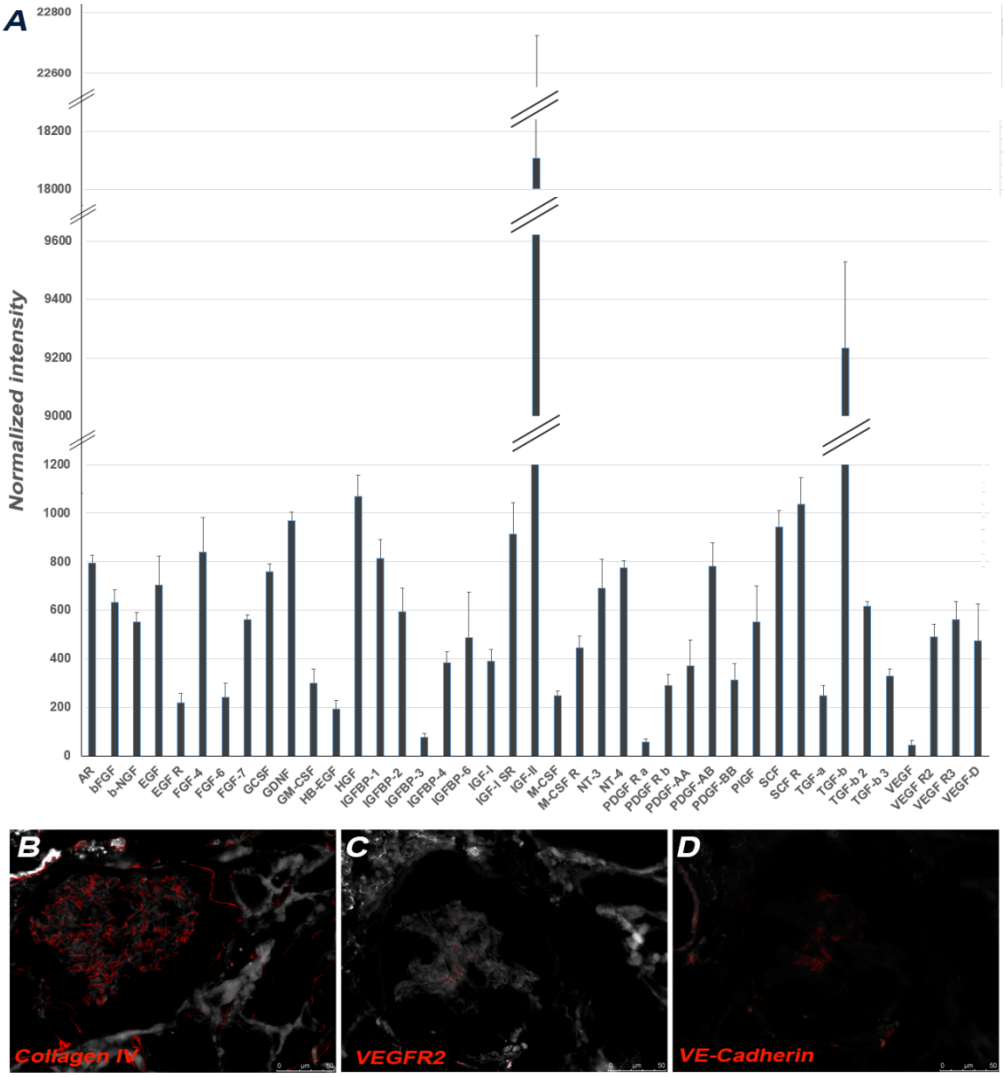

Table 1 – GFs analysis of hrECMs, before and after decellularization. Values are expressed as normalized intensity within native kidneys and scaffolds.

Human Growth Factors Array - Native kidney						
AR	**bFGF**	**b-NGF**	**EGF**	**EGF R**	**FGF-4**	**FGF-6**
438.10 ± 16.25	5585.10 ± 1363.04	462.70 ± 29.95	1576.10 ± 326.27	5360.30 ± 577.50	565.60 ± 20.19	54.10 ± 9.80
FGF-7	**GCSF**	**GDNF**	**GM-CSF**	**HB-EGF**	**HGF**	**IGFBP-1**
389.70 ± 11.84	499.80 ± 23.68	569.30 ± 29.04	402.90 ± 22.49	73.90 ± 10.36	16626.40 ± 3402.84	10023.00 ± 5834.07
IGFBP-2	**IGFBP-3**	**IGFBP-4**	**IGFBP-6**	**IGF-I**	**IGF-I SR**	**IGF-II**
2018.9 ±555.18	21.3 ± 5.72	266.1 ± 12.27	266.5 ± 20.72	346 ± 40.67	497.9 ± 8.28	63180.1 ± 1964.59
M-CSF	**M-CSF R**	**NT-3**	**NT-4**	**PDGF R a**	**PDGF R b**	**PDGF-AA**
411.7 ± 151.93	523.1 ± 169.12	252.9 ± 11.33	469.3 ± 11.83	164.5 ± 12.02	433.7 ± 21.52	554.6 ± 48.24
PDGF-AB	**PDGF-BB**	**PlGF**	**SCF**	**SCF R**	**TGF-a**	**TGF-b**
984.2 ± 138.75	641.5 ± 170.89	281 ± 14.87	496.4 ± 68.47	386.5 ± 24.35	44.9 ± 11.85	4520.8 ± 391.55
TGF-b 2	**TGF-b 3**	**VEGF**	**VEGF R2**	**VEGF R3**	**VEGF-D**	
434.9 ± 10.63	125.3 ± 10.99	28.9 ± 9.62	855.4 ± 107.12	317 ± 29.87	185.8 ± 24.84	

Human Growth Factors Array - Acellular kidney (hrECM)						
AR	**bFGF**	**b-NGF**	**EGF**	**EGF R**	**FGF-4**	**FGF-6**
753.6 ± 29.40	612.6 ± 50.56	654.3 ± 40.35	948.5 ± 116.63	255.8 ± 37.50	1051.8 ± 140.84	277.2 ± 60.52
FGF-7	**GCSF**	**GDNF**	**GM-CSF**	**HB-EGF**	**HGF**	**IGFBP-1**
500.2 ± 22.03	732.2 ± 34.15	859.1 ± 35.39	503 ± 57.59	233.3 ± 36.17	802.6 ± 88.85	791.5 ± 78.59
IGFBP-2	**IGFBP-3**	**IGFBP-4**	**IGFBP-6**	**IGF-I**	**IGF-I SR**	**IGF-II**
582.9 ± 98.18	106.7 ± 16.00	502.9 ± 44.40	905.7 ± 184.62	483.5 ± 47.51	958.4 ± 131.08	17775.2 ± 4617.7
M-CSF	**M-CSF R**	**NT-3**	**NT-4**	**PDGF R a**	**PDGF R b**	**PDGF-AA**
235.9 ± 18.84	445.2 ± 47.80	785.2 ± 121.75	713.2 ± 29.28	80.3 ± 13.56	475.4 ± 47.61	746.8 ± 108.95
PDGF-AB	**PDGF-BB**	**PlGF**	**SCF**	**SCF R**	**TGF-a**	**TGF-b**
957.9 ± 97.99	490 ± 67.16	904.6 ± 148.18	876.3 ± 67.80	929.6 ± 110.23	268.6 ± 39.50	8322.7 ± 297.22
TGF-b 2	**TGF-b 3**	**VEGF**	**VEGF R2**	**VEGF R3**	**VEGF-D**	
611.8 ± 16.95	351.1 ± 32.06	78.8 ± 17.97	542.2 ± 51.91	586 ± 76.75	538.5 ± 150.54	